Steel and Composite Structures, *Vol. 35, No. 2 (2020) 261-278*
DOI: https://doi.org/10.12989/scs.2020.35.2.261

Experimental study on steel-concrete composite beams with Uplift-restricted and slip-permitted screw-type (URSP-S) connectors

Linli Duan[1], Hongbing Chen[2], Xin Nie[*2,3] and Sanwei Han[2]

[1]College of Civil Engineering, Hunan University, Changsha 410082, China
[2]Key Laboratory of Civil Engineering Safety and Durability of China Education Ministry, Department of Civil Engineering, Tsinghua University, Beijing 100084, China
[3]National Engineering Laboratory for Green and Safe Construction Technology in Urban Rail Transit, Tsinghua University, Beijing 100084, China

(*Received July 6, 2019, Revised December 18, 2019, Accepted December 23, 2019*)

Abstract. In steel-concrete composite beams, to improve the cracking resistance of the concrete slab in the hogging moment region, a new type of connector in the interface, named uplift-restricted and slip-permitted screw-type (URSP-S) connector has been proposed. This paper focuses on the behavior of steel-concrete composite beams with URSP-S connectors. A total of three beam specimens including a simply supported beam with URSP-S connectors and two continuous composite beams with different connectors arrangements were designed and tested. More specifically, one continuous composite beam was equipped with URSP-S connectors in negative moment region and traditional shear studs in other regions. For comparison, the other one was designed with only traditional shear studs. The failure modes, crack evolution process, ultimate capacities, strain responses at different locations as well as the interface slip of the three tested specimens were measured and evaluated in-depth. Based on the experimental study, the research findings indicate that the larger slip deformation is allowed while using URSP-S connectors. Meanwhile, the tensile stress reduces and the cracking resistance of the concrete slab improves accordingly. In addition, the overall stiffness and strength of the composite beam become slightly lower than those of the composite beam using traditional shear studs. Moreover, the arrangement suggestion of URSP-S connectors in the composite beam is discussed in this paper for its practical design and application.

Keywords: steel-concrete composite beam; uplift-restricted and slip-permitted screw-type (URSP-S) connector; experimental study; cracking resistance; interface slip

1. Introduction

In largescale civil infrastructures, the steel-concrete composite structures, such as concrete-filled steel columns (Hajjar 1998, Lam and Williams 2004), composite beams (Ranzi *et al*. 2004, Nguyen and Machacek 2016), steel-concrete composite frames (Bursi and Gramola 2000, Huang *et al.* 2012), and steel-concrete composite bridges (Wegmuller and Amer 1977, Seracino *et al*. 2001), are widely employed as the primary load-bearing structural components. Due to the combination of the advantages of both steel and concrete, steel-concrete composite structure owns excellent structural performance, such as high capacity and stiffness, great seismic performance and stability, fast and convenient construction (Mirza and Uy 2010, Taranath 2011, Martinelli *et al.* 2012, Hsu *et al*. 2014, Liu *et al*. 2017).

The reliable connection between a steel beam and concrete slab is of vital importance for the co-working capability of steel-concrete composite structures. Currently, the headed stud connector and the Perfobond strip are two main traditional types of the shear connector being widely used in composite structures to realize compatible deformation of steel and concrete (Ollgaard *et al.* 1971, Oguejiofor and Hosain 1994, Ellobody and Lam 2002, Taeyang 2004, He *et al*. 2016). These types of shear connectors can efficiently prevent the separation between the concrete slab and steel beam of the composite beam, as well as transfer shear force by restricting the interface slip.

Generally, for steel-concrete composite structures under positive moment, the steel beams and the concrete slabs are subjected to tension and compression, respectively, which fully utilizes the mechanical properties of materials. However, in some structures, i.e., continuous composite bridges and frame composite beams, the concrete in composite beams will be in tension and crack may occur in the negative moment region. Cracking behavior of concrete significantly influences the performance of structures such as material strength, structural stiffness and durability (Bazant and Oh 1983, Song *et al.* 2006). This problem has always been a critical concern hindering the application and extension of steel-concrete composite structures. To solve this problem and reduce the tensile stress in the concrete slab, the prestressed technique has been widely adopted in the last few decades (Prodyot *et al.* 1987, Okumus *et al*. 2012). However, due to the compatible deformation between steel and concrete, most of the prestress applied to the composite beam is undertaken by the steel beam, which

∗Corresponding author, Assistant Professor
E-mail: xinnie@tsinghua.edu.cn

http://www.techno-press.org/?journal=scs&subpage=8
ISSN: 1229-9367 (Print), 1598-6233 (Online)

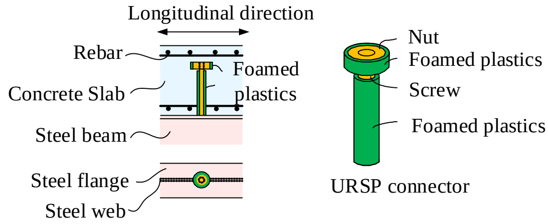

Fig. 1 URSP-S connector

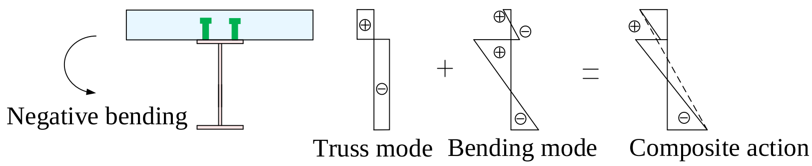

Fig. 2 Stress and strain analysis of a composite beam section under hogging moment

means that the prestressed technique has a high-stress loss in composite structures. Moreover, the construction process of the prestressed technique is very complex and time-consuming.

To lower the tensile stress and postpone the cracking of concrete slab, another effective method to release the shearing force between steel and concrete was proposed. A new type of connector, named the uplift-restricted and slip-permitted (URSP) connector, including T-shape connector (URSP-T) and screw-type connector (URSP-S), was proposed by Nie *et al*. (2015). Owing to the obvious advantages, including the simple structural detail, low cost and construction convenience (Nie *et al.* 2019), the URSP-S connectors are adopted for the tested composite beams in this study, as illustrated in Fig. 1. The screw and the nut keep its original construction features of stud connectors and are enclosed with foamed plastics. Therefore, the URSP-S connectors can still restrict the uplift of the concrete slab from the steel beam, and permit the interface slip between the concrete slab and steel beam. Therefore, the shear force at the interface is released and the tensile stress in the concrete slab can be reduced.

The experimental and numerical studies on the performance of the URSP connectors have been reported in recent years. Pushout and pullout tests were conducted to investigate the slip and uplift performance of URSP-T connectors, and a hysteresis model was proposed to effectively simulate the mechanism characteristic of URSP connectors (Nie *et al*. 2015). The mechanical performance of USRP-T connector with foamed plastics in overhanging three-span composite girders has been reported by Li *et al.* (2019). The shear-slip curve of URSP-S connector was proposed in previous studies (Han 2016, Duan *et al.* 2019). The detailed characteristics corresponding to different loading stages have been discussed in depth as well, which is omitted in the study. Practical design guidelines and construction methods were put forward for the application of URSP-S connectors in a three-span continuous composite bridge (Li *et al.* 2017). The effect of URSP-S connectors on the stiffness, strength and cracking performance in the composite frame was numerically investigated (Duan *et al.* 2019). However, the structural performance of composite structures with URSP-S connectors has not been experimentally investigated until now.

In this study, the structural behavior of composite structures with URSP-S connectors in the region of negative moments was systematically evaluated. Firstly, the mechanism of the composite beam with URSP connectors was investigated. Then, the experimental program, test results and analysis were described and discussed in detail. Besides, the arrangement suggestion of URSP-S connectors in the composite beam was provided, which is significant to promote the practical applications of URSP-S connectors in the future civil engineering structures.

2. Mechanism of composite beam with URSP connectors

Flexible connectors, such as studs, will deform when transferring shear force between the steel beam and concrete interface, which will cause slip deformation at the interface. Under a negative bending moment, the stress and strain of the composite section considering the interface slip behavior can be divided into truss mode and bending mode (Dezi *et al.* 2001), as depicted in Fig. 2. In the truss mode, due to the shear force at the steel-concrete interface provided by shear connectors, the concrete slab and steel beam are subjected to axial tension and compression, respectively. While in the bending mode, the bending behavior of concrete slab and steel beam are considered, and the two components behave as two independent beam elements with individual neutral axes. When URSP connectors are applied in regions of negative bending moment of a composite beam, the longitudinal constraint along the span direction at the steel-concrete interface is released. Due to the fact that the contribution of truss mode is proportional to the degree of shear connection (Betti and Gjelsvik 1996), the truss mode can be neglected, and only the bending mode is taken into consideration. Therefore, the

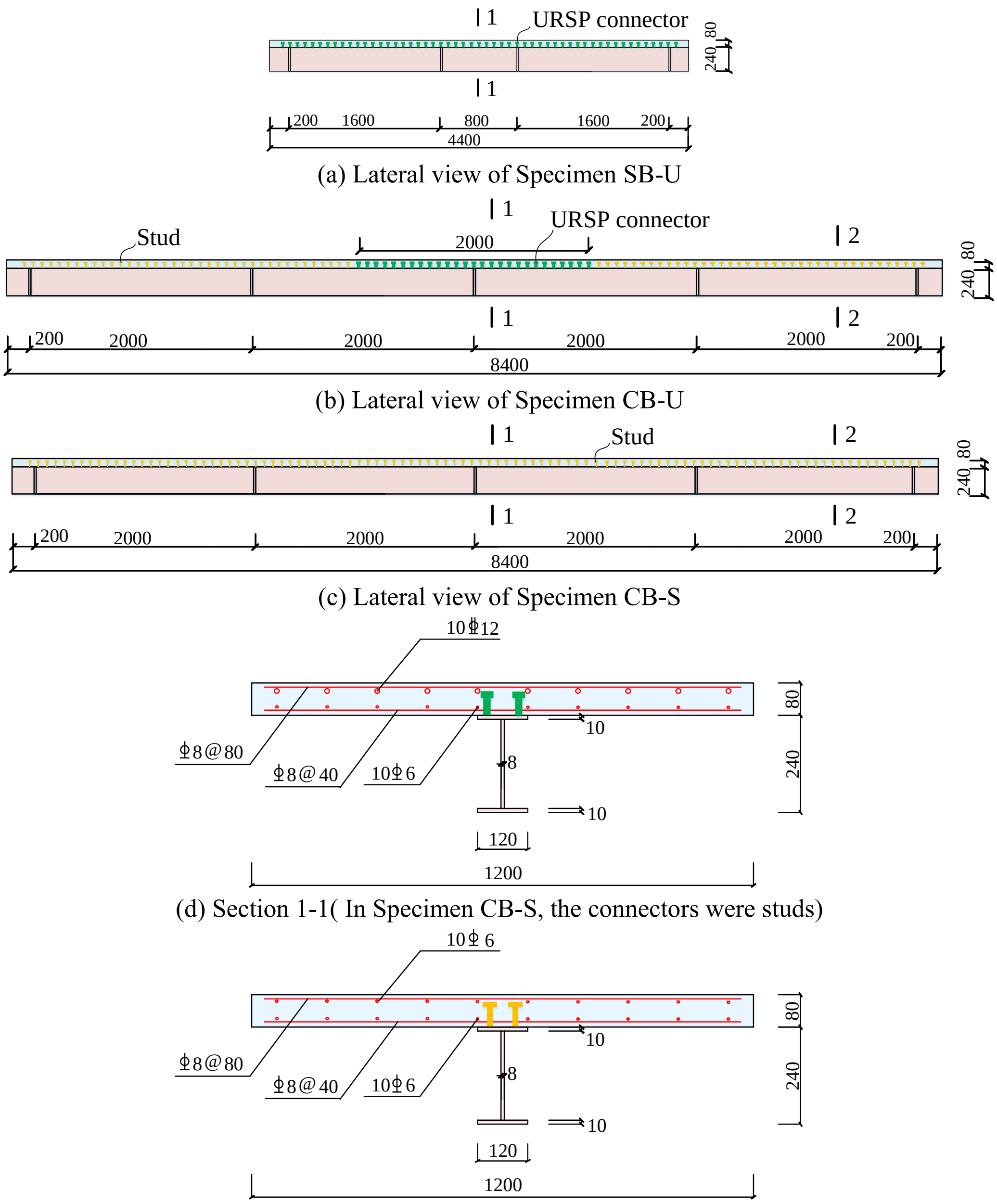

(a) Lateral view of Specimen SB-U

(b) Lateral view of Specimen CB-U

(c) Lateral view of Specimen CB-S

(d) Section 1-1(In Specimen CB-S, the connectors were studs)

(e) Section 2-2

Fig. 3 Specimens of beam tests (unit: mm)

tensile stress and strain of concrete slab can be sharply decreased in regions of negative bending moment of a composite beam (Abe and Nakajima 1990).

It has been reported that conventional shear connectors (welded studs) usually induce concentrated forces inside the concrete slab and hence create splitting cracks or crushing cracks (Johnson 2004). Suwaed and Karavasilis (2017, 2018) proposed a novel demountable shear connector with large slip capacity, which can release the stress concentration and possess great strength and stiffness. While using URSP connector wrapped with plastic foam, the stress concentration can also be alleviated.

After applying the URSP connectors in the hogging moment region of composite beams, the tensile stress and strain of concrete slab are significantly reduced. However, the structural behavior of steel-concrete composite beams with URSP connectors in the interface should be systematically investigated, for further promoting the practical application of URSP connectors in steel-concrete composite structures.

3. Experimental program

3.1 Specimen design

According to the plastic design method in the Chinese code for design of composite structures (2016), three

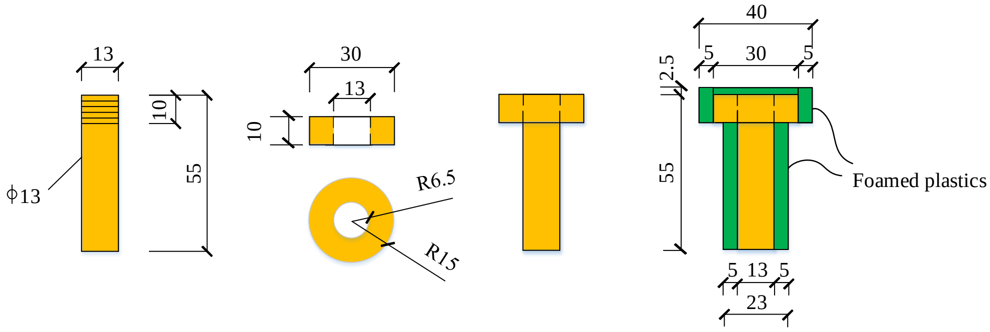

(a) Dimension details of URSP-S connector (unit: mm)

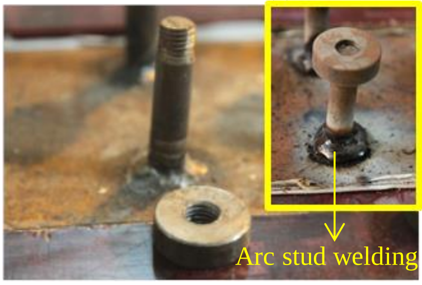

(b) Screw and nut

(c) Wrap the nut with the foamed plastics

(d) Wrap the screw with the foamed plastics

(e) Tighten the screw and nut

Fig. 4 Installation details of URSP-S connector

specimens, including a simply supported beam under negative loading and two two-equal-span continuous beams under loading at mid-span, were designed and tested. To investigate the behavior of composite beams with URSP-S connectors, including the capacity, flexural stiffness, slip between the slab and steel beam and the evolution process of the crack in the concrete slab, the simply supported beam was arranged with URSP-S connectors along the whole beam, designated as Specimen SB-U. The two continuous beams, one of which was arranged with studs only and the other with URSP-S connectors near middle support (1000 mm on both sides of middle support) while studs in other regions, were labeled as Specimens CB-U and CB-S, respectively. According to the elastic solution calculated by structural mechanics, the negative bending moment zone was located within the range of 1.091 m on both sides of the middle support. With the plastic development of the composite beam, the negative moment region would decrease accordingly. Therefore, the regions of 1.0 m on both sides of middle support were arranged with URSP-S connectors in Specimen CB-U.

Figs. 3 and 4 show the lateral and sectional view of three beams and detailed construction features of the URSP-S connector. The sectional view 1-1 depicted in Fig. 3(d) reinforces the concrete slab in Specimen SB-U, as well as the slab of negative moment region in Specimens CB-U and CB-S. The sectional view 2-2 of reinforcement in positive moment region in Specimens CB-U and CB-S is also given in Fig. 3(e). The only difference between the two sections is the diameter of longitudinal reinforcement at the upper layer of the slab. The actual concrete cover was between 15 mm and 20 mm, which was in accordance with the specification in the Chinese code for design of concrete structures (2010). In order to prevent the steel beam from buckling at the support and the loading point, the vertical stiffeners with thicknesses of 16 mm were arranged on both sides of the steel beam web at each support and loading point. In all specimens, shear connectors were arranged in two rows with a longitudinal and lateral spacing of 80 mm and 67 mm, respectively, which were designed based on the full composite shear connection in the Chinese code for design of composite structures (2016). For normal studs, the diameter and the height were 13 mm and 55 mm,

Table 1 Material properties of concrete

Specimen	Compressive strength f_{cu} (MPa)	Compressive strength f_c' (MPa)
SB-U	42.1	32.0
CB-U CB-S	37.7	28.7

Table 2 Material properties of steel plate and reinforcement

Type of steel	Yield strength (MPa)	Ultimate strength (MPa)
8 mm steel plate	289.0	445.9
10 mm steel plate	277.5	425.3
12 mm reinforcement	455.0	614.0
6 mm reinforcement	436.0	664.0
8 mm reinforcement	345.0	537.0

respectively. The construction and machining process of URSP-S connectors are presented in Fig. 4. The URSP-S connectors were composed of screw and nut. The diameter and the height of the screw were the same as those of studs. The screw thread was set within the top 10 mm range. The thickness of the nut was 10 mm, the outer diameter was 30 mm. The inner diameter was 13 mm, which was the same as the diameter of the screw. The screw thread was set in the nut to connect with the screw. The exterior dimension of the URSP-S connector was almost the same as that of the stud. The foamed plastics were used to wrap the nut and screw separately, and then the screw and nut were tightened together. The reason using a screw and a nut rather than a standard stud as a URSP-S connector is due to the manufacture convenience of the URSP-S connector.

3.2 Material properties

The concrete grade was C30, with a nominal cubic compressive strength of 30 N/mm^2. According to the Chinese standard for test method of mechanical properties on ordinary concrete (2016), the mechanical properties of concrete in the composite specimens were measured through material property tests performed on the same day of each loading test. The concrete compressive strength associated with cubes and prisms, f_{cu} and f_c', were determined respectively, as shown in Table 1. The Q235 steel with nominal strength of 235 MPa was used for the steel plate, based on Chinese metallic materials-tensile testing-method of test at ambient temperature (2010), material properties of steel and reinforcements including yield strength and ultimate strength are listed in Table 2. The shear connectors were produced and processed in strict accordance with relevant standards (Chinese cheese head studs for arc stud welding (2002), Chinese steels for cold heading and cold extruding (2015)). According to these Chinese codes, the tensile strength should not be less than 400 N/mm^2, and the yield strength should not be less than 320 N/mm^2. The steel beams of each test piece were made of welded I-beam and manufactured in steel structure factory. The shear connectors were welded on the steel beam. Then the steel beam was transported to the laboratory and the concrete slabs were poured and cured here for 28 days.

3.3 Test setup and instrumentation

Due to the limitation of laboratory conditions, the simply supported beam was upside down tested for negative loading, as shown in Fig. 5(a). A distribution beam was used to distribute the load applied by a 100-ton hydraulic jack along the width of the specimen at each loading point. Roller bearings were used at one end of the support, and triangular bearings were arranged at the other end to form the simply support condition.

In the case of continuous beams, the load was applied by a 100-ton hydraulic jack through transversely distributing beams in the middle of each span, as shown in Fig. 5(b). Since Specimens CB-U and CB-S were statically indeterminate, the force cell and screw jack were placed at every support. Before the loading of the test, the initial interior force in the continuous beam could be eliminated by adjusting the screw jacks. The beam was supported by two rollers at the ends and one pin in the middle. The longitudinal movements of the beam ends were not restricted, for avoiding internal force in these continuous beams.

During the loading process, the multi-stage loading method was adopted to prevent the brittle failure of the structure. In the initial stage of loading test, the load was applied with force control approach, the load increment was set to 5 kN (simply supported beam) or 10 kN (continuous beam) per step. For simply supported beam, the load increment was adjusted to 10 kN per step after the load reached half of the expected ultimate load(220 kN /2=110 kN), which was calculated according to the plastic design method for full composite shear connection cases in the Chinese code for design of composite structures (2016). When the structure entered the plastic stage where the load-deflection curve had a significant inflection point, the external load was gradually applied using displacement control until the structural failure.

Fig. 6 presents the detailed arrangement of the measuring devices attached to each specimen. Each

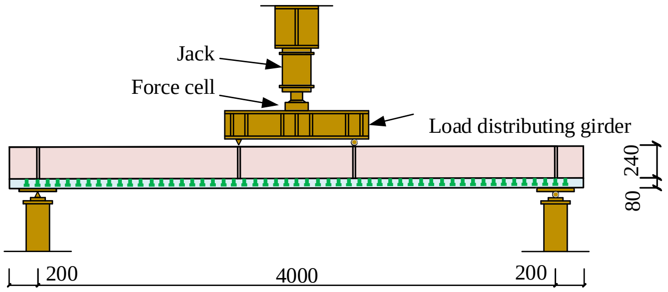

(a) Specimen SB-U

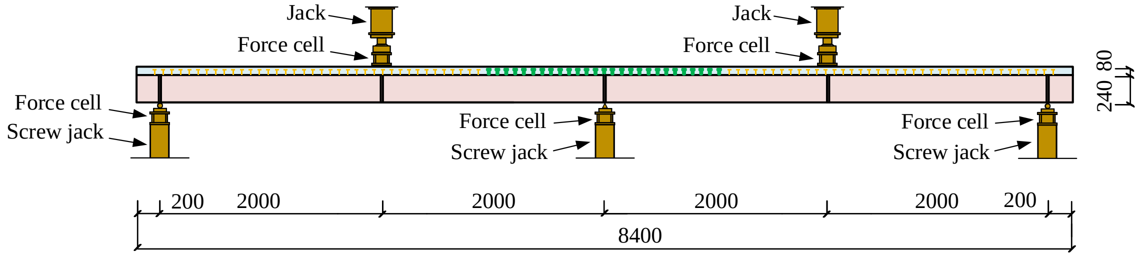

(b) Specimens CB-U/CB-S (In Specimen CB-S, the connectors were studs)

Fig. 5 Loading systems of tested specimens (unit: mm)

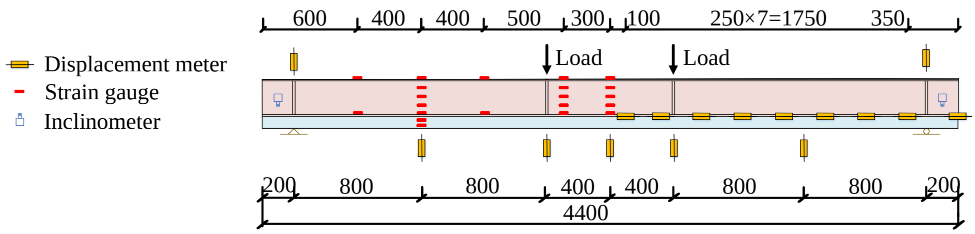

(a) Elevation of Specimen SB-U

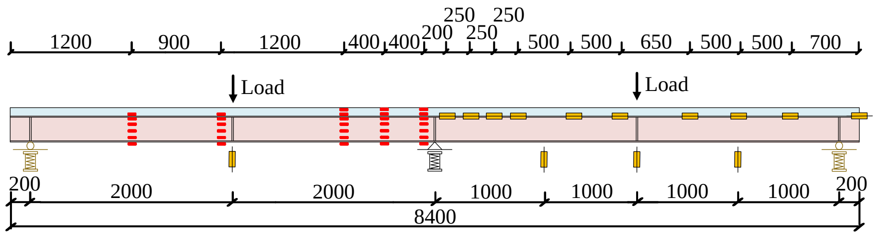

(b) Elevation of Specimens CB-U/ CB-S

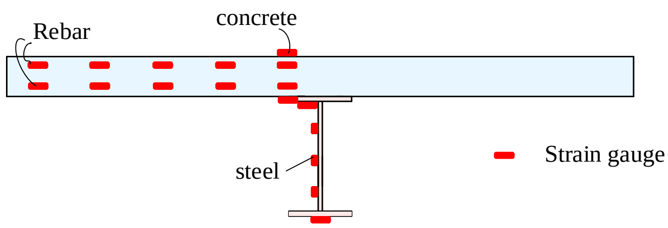

(c) Cross-section of Specimens SB-U/CB-U/CB-S

Fig. 6 The arrangement of measurement devices of tested specimens (unit: mm)

specimen was instrumented to record the following response: the strain on the concrete slab and steel girder, the angle of rotation, the deflection of the girder, as well as the relative slip between the concrete slab and steel girder. The slip was measured by displacement meter connected with two guide bars, which were separately attached to the concrete slab and steel beam. The type of displacement meter was YHD. The resistance strain gauges for concrete

(a) Specimen SB-U before the test

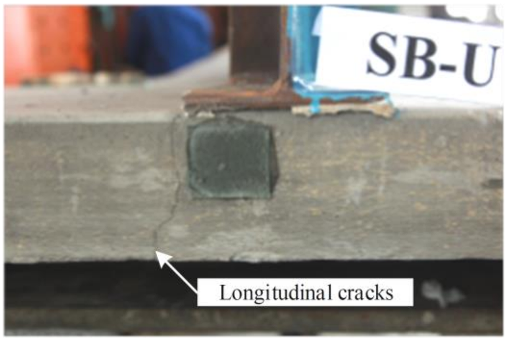

(b) Longitudinal cracks on the north side of the concrete flange plate

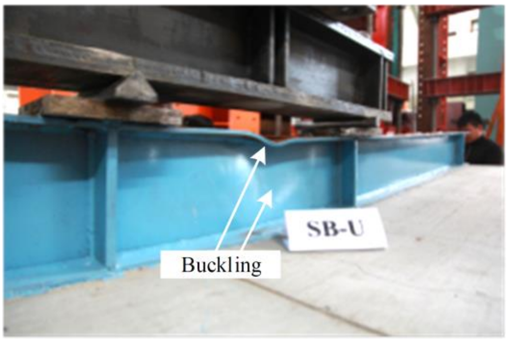

(c) Buckling of lower flange and web of steel beams

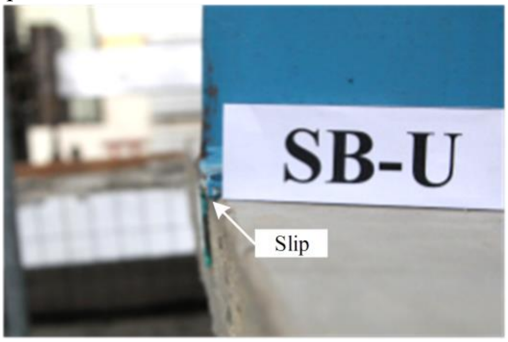

(d) Slip between the steel beam and concrete slab

Fig. 7 Experimental observations from tested Specimen SB-U

slab and steel beam were S2120-80AA and BX120-3A A, respectively.

4. Experimental results and analysis

4.1 Test observations

Experimental observations of the tested Specimen SB-U are presented in Figs. 7(a)-7(d). The tested Specimen SB-U maintained the linear behavior and the stiffness of the beam kept constant in the initial loading stage. When the load increased to a relatively low load of 20 kN, the first visible crack was observed. While loading to 45 kN, obvious sound in the interface between the concrete slab and steel component could be heard, the maximum slip was only 0.15 mm, which indicated the bonding of the steel-concrete interface was broken and the interface slip occurred. At the service limit states, the initial vertical stiffness of composite beams decreased slightly due to the effect of the URSP-S connectors (Duan *et al.* 2019). However, the maximum crack width decreased accordingly. When the load was between 0.8 P_u and P_u, the longitudinally tensioned steel bars and the lower flanges of the steel beams almost yielded simultaneously. Cracks in concrete slab began to develop rapidly, and most of the cracks became through cracks.

At the time instant when the load reached the ultimate load P_u, the lower flange and the web of the steel plate were buckled. Meanwhile, the deflection evolution of the composite beam was further accelerated and the reaction force began to decrease slowly, which indicated that the composite beam exhibited excellent ductility. Concurrently, a small number of longitudinal cracks appeared in the concrete slab near the ends of the beam, as shown in Fig. 7(b).

However, the development of longitudinal cracks was small and it was only observed near the end of the beam. Therefore, the longitudinal cracks were not the controlling factor for the bending failure of the composite beam. At the final loading stage, the buckling degree of the lower flange and web of the steel beam was increased, and it can be considered that the composite beam had reached its damage limit. The buckling phenomenon of the steel plate is shown in Fig. 7(c). After the unloading procedure was completed, the obvious relative slip was observed at the interface between the steel beam and the concrete slab at both ends of the composite beam, as exhibited in Fig. 7(d).

The test setup, global deflection, steel buckling and crushing failure pattern of the tested continuous beams CB-U and CB-S are presented in Figs. 8(a)-8(d). It was observed that the first crack appeared both in Specimens CB-U and CB-S while the load reached 20 kN. At this loading stage, the concrete had reached the cracking stress while the interface had not been broken, the effect of URSP-S connectors in Specimen CB-U was not significant. The deflected shapes of the Specimens CB-U and CB-S were similar at the final loading stage, as shown in Fig. 8(b). The failure modes of Specimens CB-U and CB-S were induced by the buckling of the lower flange of the steel beam at the middle support, as shown in Fig. 8(c). At the same time, the plastic hinge was observed at the middle loading point of the south span of the composite beam, and the deflection increased rapidly and eventually led to the

(a) Specimen before the test

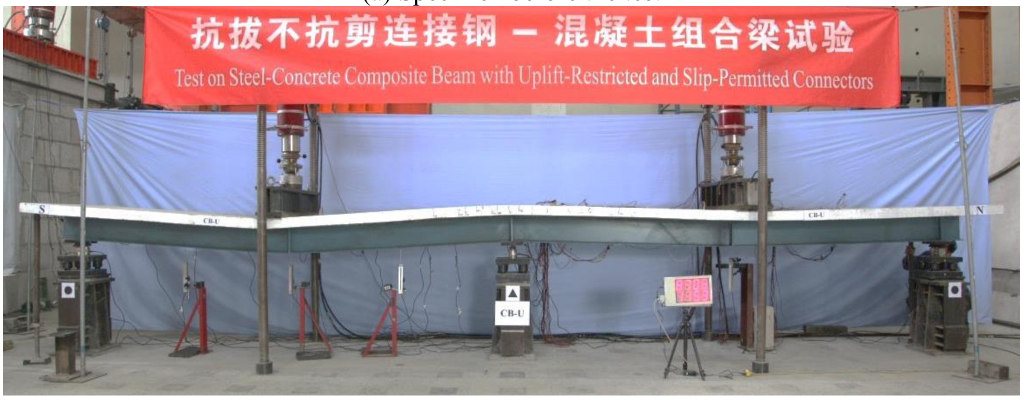

(b) Global deflection of Specimen after loading test

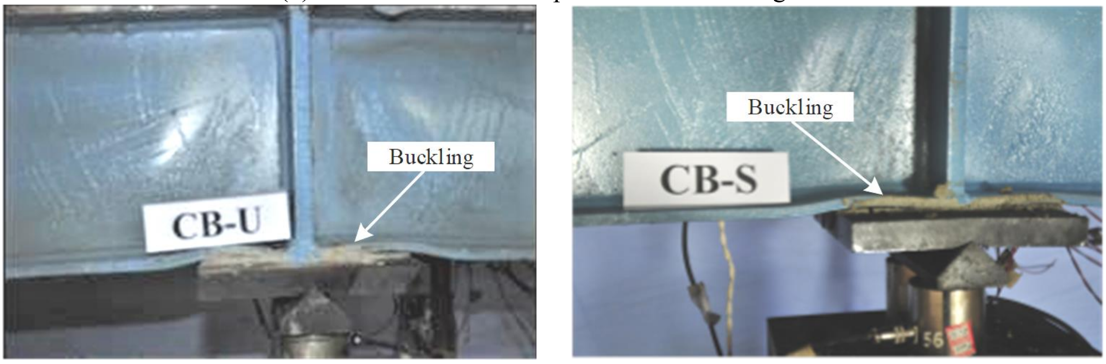

(c) Buckling of the lower flange of steel beam at middle support

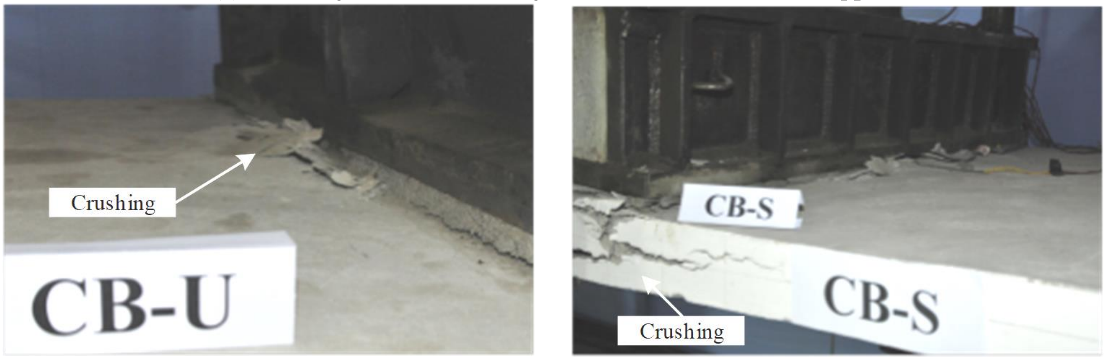

(d) Crushing failure of the concrete slab

Fig. 8 Experimental observations from tested Specimens CB-U and CB-S

collapse of the concrete, as exhibited in Fig. 8(d). The failure mode of Specimen CB-S was very similar to that of Specimen CB-U. The only difference could be observed was the specific location where the failure occurred.

4.2 Load versus deflection curves

The load-displacement curves of Specimens SB-U, CB-U and CB-S are illustrated in Figs. 9(a) and 9(b),

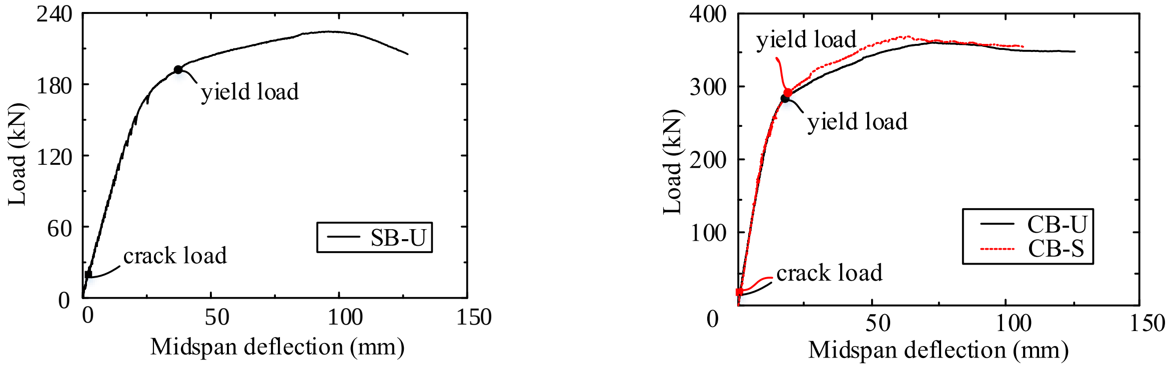

(a) Specimen SB-U (b) Specimens CB-U and CB-S

Fig. 9 Load versus deflection curves

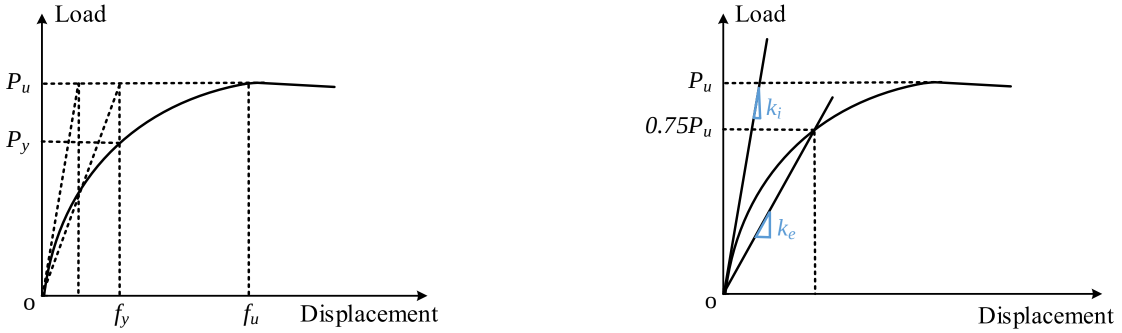

(a) Yielding points (P_y, f_y) (b) Initial stiffness K_i and effective stiffness K_e

Fig. 10 Determinations of P_y, f_y, K_i and K_e

Table 3 Summary of test results

Specimen	Crack load P_c (kN)	P_c / P_u	Yield Load P_y (kN)	P_y / P_u	Ultimate load P_u (kN)	Yield deflection f_y (mm)	Ultimate deflection f_u (mm)	f_u / f_y	Initial stiffness K_i (kN/mm)	Effective stiffness K_e (kN/mm)
SB-U	20	0.090	198	0.887	223	32.2	97.6	3.031	9.4	6.6
CB-U	20	0.056	288	0.800	360	19.7	73.8	3.746	24.6	17.8
CB-S	20	0.054	293	0.796	368	20.1	60.6	3.015	25.1	16.8

respectively. In the initial loading stage, the surficial strains corresponding to the concrete slab and steel beam in Specimen SB-U were relatively small, the specimen maintained the linear behavior and the structural stiffness of the beam kept identical in this stage, as presented in Fig. 9(a). After reached the crack load, the load versus deflection relationship entered the elastic-plastic stage. When loaded to the yield load, the structural stiffness of the composite beams decreased sharply. Meanwhile, the increasing rate of the reaction force was greatly decelerated and the deflection was rapidly increased. At this time instant, the load-displacement curve presented an obvious inflection point.

For Specimens CB-U and CB-S, the load-displacement curves also exhibited three typical stages, as shown in Fig. 9(b). The relationship between load and displacement of the tested Specimens CB-U and CB-S were similar at the elastic and elastic-plastic stages. The initial stiffness of Specimen CB-S was slightly larger than that of the Specimen CB-U, but the effective stiffness was lower due to the concrete cracking. After entering the plastic stage, the stiffness of Specimen CB-U was slightly lower than that of Specimen CB-S. However, the yield loads and ultimate loads of the two specimens were quite close. It has been proved that the contribution provided by concrete slab and the composite action was significant to the structural performance of steel-concrete composite beams (Liang *et al.* 2004). The experiment results in this study indicate that the arrangement of the URSP-S connectors in hogging moments barely affects the ultimate strength, which guarantees the composite action between the concrete slab and steel beam and the excellent mechanical performance of composite beams.

The values of load, deflection, the P_c / P_u and P_y / P_u ratios, the ductility coefficient f_u / f_y of Specimens SB-U, CB-U and CB-S are summarized in Table 3. It should be noted that the crack load P_c is the loading level corresponding to the appearance of the first crack. The ultimate load P_u is the maximum load before structural failure and the ultimate deflection f_u corresponds to the

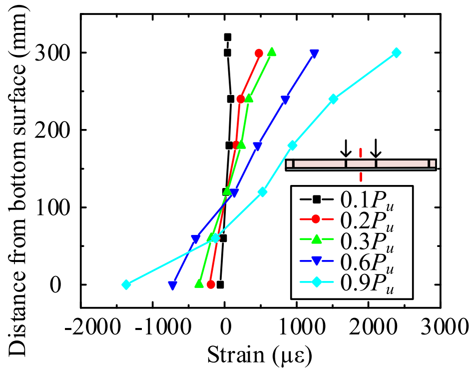

(a) Mid-span section

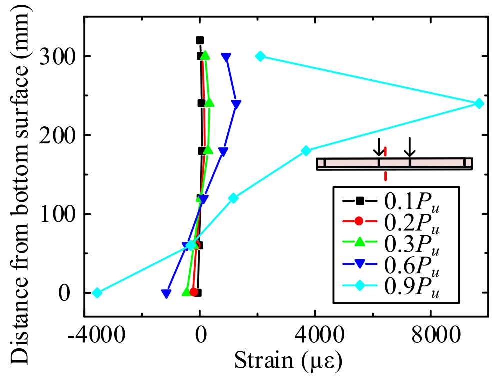

(b) Section near the boundary of the pure bending region

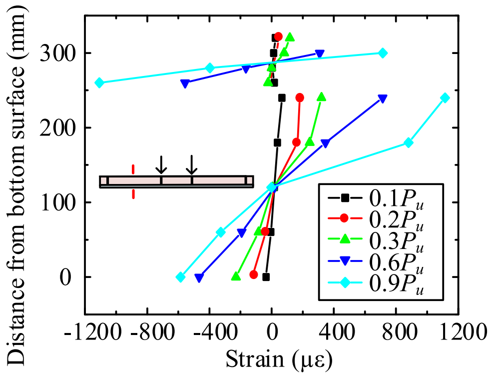

(c) Mid-span section of the shear span

Fig. 11 Vertical strain distribution of different sections in Specimen SB-U

ultimate load. The yield point (P_y, f_y) in the load-deflection curve can be determined using the graphical method described by Liu *et al.* (2015), as shown in Fig. 10(a). The initial stiffness is defined as the tangent slope at the origin point of the load-displacement curve, and the effective stiffness of the beam can be calculated as per the experimental study performed by Park and Thompson (Park and Thompson 1974). The detailed information on the determination of the initial stiffness K_i and effective stiffness K_e is illustrated in Fig. 10(b).

4.3 Strain analysis at the critical sections

The strain distribution was measured with the strain gauges attached to the outer surface of the tested specimens at the critical sections. As presented in the aforementioned Fig 3, the height of the steel beam was 240 mm. Therefore, the strain gauges with heights of zero mm and 240 mm were arranged at the lower and upper flanges of the steel beam, respectively. The strain gauges with heights of 60 mm, 120 mm and 180 mm were located on the webs of the steel beams. In addition, the strain gauges with heights greater than 240 mm were designed for observing the strain of concrete and steel reinforcement. In the Specimen SB-U, the distribution curves of the longitudinal strain along the section height of three typical sections are shown in Fig. 11. It can be seen from the experimental observations presented in Fig. 11 that the strain distributions of the three cross-sections of the Specimen SB-U subjected to the negative moment induced by the load smaller than 0.2 P_u were almost consistent with that of the plane cross-section assumption. When the load reached 0.2 P_u, the steel-concrete interface was broken and the interfacial slip occurred, strain distribution curves of mid-span section of the shear span gradually tended to deviate the prediction based on the plane cross-section assumption.

According to effective data, it can be seen from Fig. 11(a) that the strain distribution for the mid-span section matched well with that of plane cross-section assumption. For the strain distribution of the section near the boundary of the pure bending region, as shown in Fig. 11(b), the steel beam and concrete slab began to deform respectively and a significant difference was observed between the strain of rebar in the concrete slab and the top flange of the steel beam, especially for higher loading level. For the strain distribution of the mid-span section in shear span illustrated in Fig. 11(c), the strain distributed by respective neutral axes corresponding to the steel beam and the concrete slab, resulting in larger interface slip. It should be mentioned that parts of the strain data were not obtained due to the damage of strain gauges led by the severe cracking in concrete slabs.

In Specimens CB-U and CB-S, the strain distribution curves in the section near the middle support of the tested two continuous beams are shown in Figs. 12(a) and 12(b), respectively. Since a relative larger interface slip strain on the steel-concrete interface was observed, the Specimen CB-U showed an obvious "non-combination" performance.

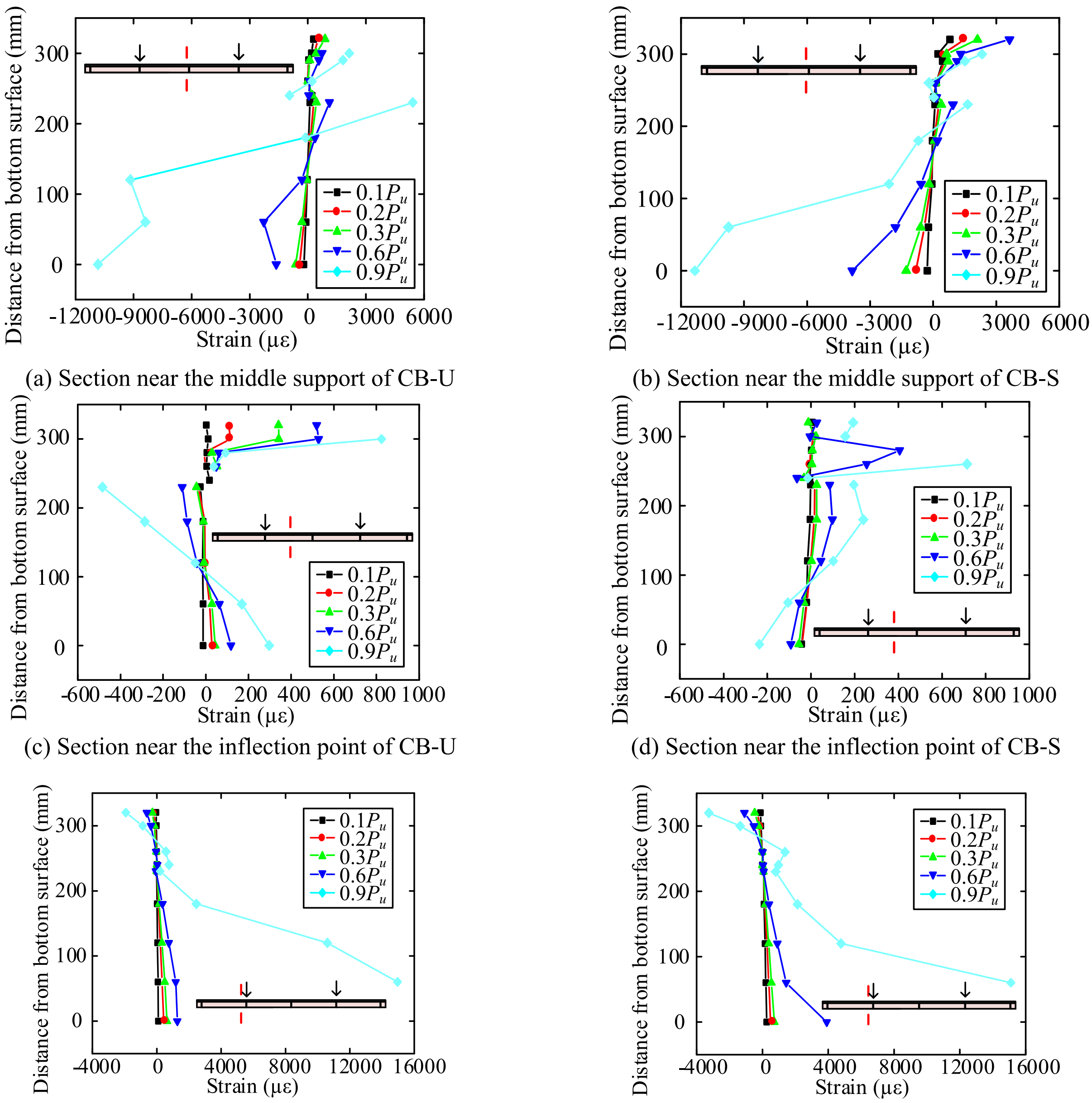

(a) Section near the middle support of CB-U

(b) Section near the middle support of CB-S

(c) Section near the inflection point of CB-U

(d) Section near the inflection point of CB-S

(e) Section near the loading point of CB-U

(f) Section near the loading point of CB-S

Fig. 12 Vertical strain distribution of different sections in Specimens CB-U and CB-S

Moreover, the strain distributed according to the neutral axes of concrete slab and steel beam respectively. As mentioned in Section 2, the tensile strain on the upper surface of the concrete slab was small and its evolution process was slow due to the thinner thickness of the concrete slab. However, the Specimen CB-S presented a strong combination effect, resulting in larger tensile strain with rapid development tendency on the upper surface of the concrete slab. Accordingly, it was more likely to form tensile cracks at the top surface of the concrete slab. In addition, the crack width and propagation also developed faster after the occurrence of the first crack.

For the section near the inflection point, the strain distribution curves are shown in Figs. 12(c) and 12(d). In general, the strain responses corresponding to Specimens CB-U and CB-S were quite different. In Specimen CB-U, the upper part and the lower part of the steel beam were subjected to compression and tension, respectively. In the section near the inflection point, the Specimen CB-U was subjected to positive bending moment. Conversely, the Specimen CB-S was under the action of negative bending moment. Therefore, the inflection point was closer to the middle support in Specimen CB-U than that of Specimen CB-S, which led to the decrement of structural stiffness and internal force redistribution in Specimen CB-U. Moreover, large slip strain was observed in this section of Specimen CB-U due to the application of URSP-S connectors.

However, the strain distribution curves in the section near the loading point of Specimens CB-U and CB-S were similar, as shown in Figs. 12(e) and 12(f). The composite beams were subjected to a positive bending moment, and both Specimens CB-U and CB-S were equipped with

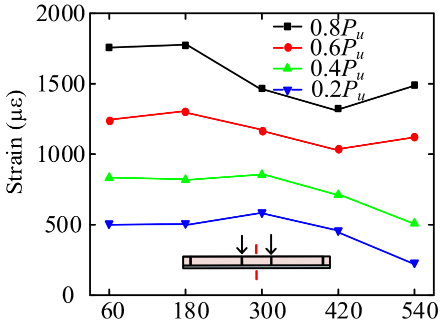

(a) Mid-span section

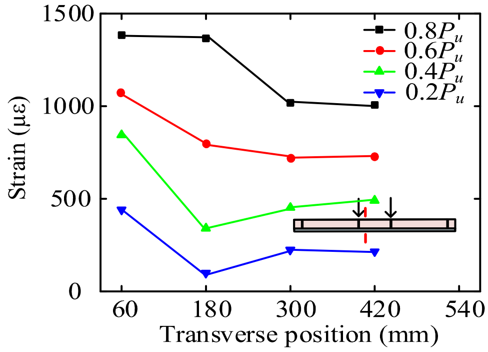

(b) Section near the boundary of the pure bending region

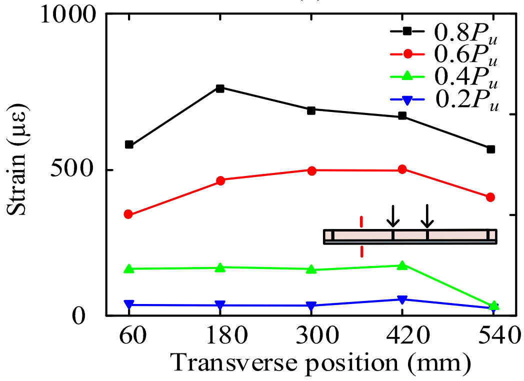

(c) Mid-span section of the shear span

Fig. 13 Lateral strain distribution of longitudinal reinforcement of Specimen SB-U

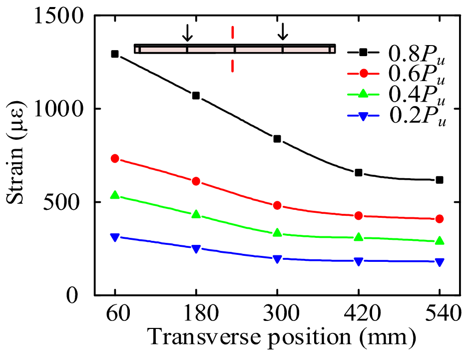

(a) Specimen CB-U

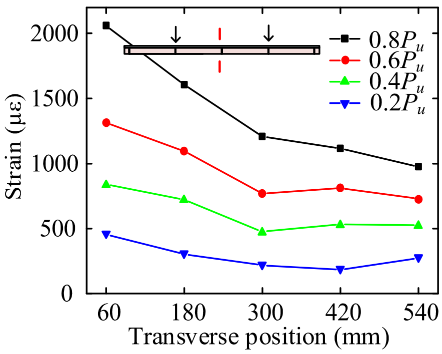

(b) Specimen CB-S

Fig. 14 Lateral strain distribution of longitudinal reinforcement of Specimens CB-U and CB-S

ordinary stud connectors in this region. The similarity of Figs. 12(e) and 12(f) shows that the application of URSP-S connectors in other regions did not affect the sectional strain distribution where stud connectors were used. In addition, according to the vertical strain distribution curves presented in Figs. 12(e) and 12(f), it is observed that the sections near the loading point exhibited integral neutral axes and the overall slip strain became smaller.

As is known, the shear lag effect mainly affects the effective width of the concrete slab in steel-concrete composite beams. In order to measure the difference of rebar strain in the lateral direction, strain gauges were arranged along the lateral direction of the longitudinal rebar at different sections including the middle section, the section near the boundary of pure bending region and the middle section of the shear span, respectively. Fig. 13 shows the measured strain distributions along the transverse direction of the longitudinal rebar in each section. The transverse position of the strain gauge started from the center of the concrete slab. Due to the geometric symmetry of tested specimens, only half of the concrete flanges were embedded with strain gauges. In the section near the boundary of the pure bending region, the effective strain data in the transverse position of 540 mm were not acquired because of the damage of strain gauges.

It can be seen from Figs. 13(a) and 13(c) that the strain of the steel-concrete composite beams with URSP-S connectors under negative bending moments was basically uniformly-distributed along the width direction of the lateral section. As shown in Fig. 13(b), for the section near

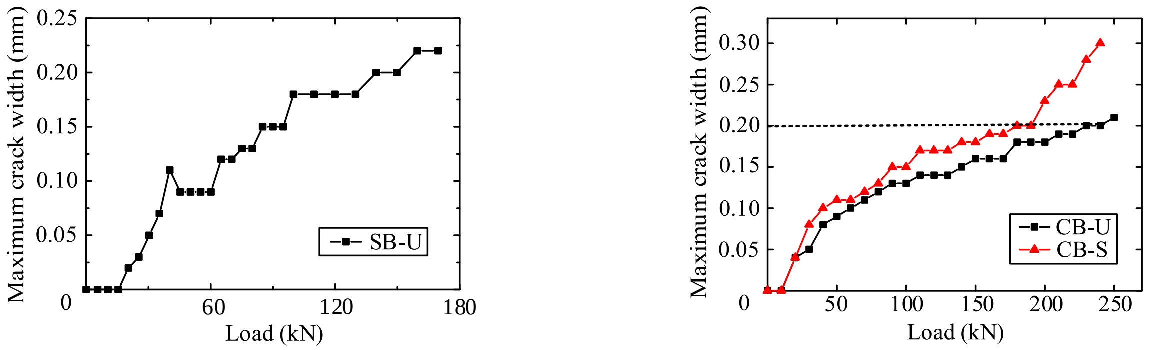

(a) Specimen SB-U (b) Specimens CB-U and CB-S

Fig. 15 Crack width of tested specimens

the boundary of the pure bending region, the strain of the longitudinal reinforcement along the transverse position was slightly different since the strain gauges were arranged near the loading point of the concentrated force. Generally, the phenomenon of shear lag was not obvious, which indicates that each longitudinal rib in concrete slab can fully exert its tensile strength. Hence, the full slab width is adopted for calculating the effective width of the concrete slab for Specimen SB-U.

In Specimens CB-U and CB-S, the strain gauges were arranged along the lateral direction of the longitudinal rebar at the section near the middle support. It can be seen from Fig. 14 that the overall strain distributions of these two specimens were similar, but the tensile strain of longitudinal reinforcement in Specimen CB-U was smaller than that of the Specimen CB-S due to the application of the URSP-S connectors. In addition, the shear lag effect was insignificant when the load was lower than $0.8P_u$. Therefore, it can be concluded that the longitudinal reinforcement in the negative bending fully exerted its tensile strength as well.

4.4 Cracking analysis

The measured maximum crack width-load curve is illustrated in Fig. 15. In Specimen SB-U, the first visible crack was observed while loading to 20 kN. The maximum crack width decreased when the interface was broken. At the same time, the interface slip increased and the URSP-S connectors began functioning accordingly. When the load reached 110 kN (about 0.5 P_u, normally considered as a load of serviceability limit), the maximum crack width was about 0.17 mm, which was still less than 0.2 mm. The maximum crack width reached 0.2 mm at a load of 0.63 M_U and it did not exceed 0.22 mm until entering the plastic stage. During the crack evolution process of Specimen SB-U, it was observed in the test that several cracks presented crack retraction with the increase of loads. The cracking phenomenon in Specimen SB-U indicated that crack development had been delayed and the crack resistance performance had been improved owing to the application of URSP-S connectors. As can be seen from Fig. 15(b), the crack development speed in the Specimen CB-U was slower than that of the Specimen CB-S, and the applied loads corresponding to crack width of 0.2 mm for Specimen CB-U and CB-S were 230 kN and 180 kN, respectively. Compared with Specimen CB-U, the crack development speed in Specimen CB-S was relatively faster. When the crack width reached 0.2 mm, the crack evolution velocity began speeding up and finally reached 0.3 mm before entering the plastic stage (0.65 *Pu*).

Since the comparison of the crack performance of composite beams with and without URSP-S connectors is crucially important, the crack distributions of Specimens CB-U and CB-S are detailly analyzed in the following sections.

As mentioned above, the concrete slab in the positive bending moment region of the composite beam was mainly subjected to compressive stress. The initiation and development process of cracks in the negative moment region of the composite beam near the middle support will be discussed below. As mentioned in Section 3.1, URSP-S connectors were arranged in the negative moment region, which was within 1.0 m from both sides of the middle support in Specimen CB-U. Therefore, it was mainly concerned with the development of cracks within 1.0 m of from both sides of the middle support.

Figs. 16(a)-16(d) show the crack distribution of concrete slabs in the tested continuous beams tests at different loading stages. More cracks were observed in the Specimen CB-S and the crack distribution was denser than that of the Specimen CB-U. Due to the influence of concrete shrinkage and hoisting construction, all the tested Specimens presented initial cracks at different levels. However, there were only a few cracks in the Specimen CB-U and the region with initial cracking region was quite small. Comparatively, more initial cracks can be observed in the Specimen CB-S. Moreover, the crack development range was larger, which indicated that the URSP-S connectors could release the tensile stress of concrete slab induced by the concrete shrinkage and component hoisting. The occurrence of cracks in the Specimen CB-S mainly emerged before the load reaching 120 kN. Then, the number of new cracks did not increase obviously, but the crack width was apparently developed. In contrast, the crack development in Specimen CB-U was relatively slower and it was basically consistent at each loading stage, which also implies that the application of the URSP-S connectors can postpone the

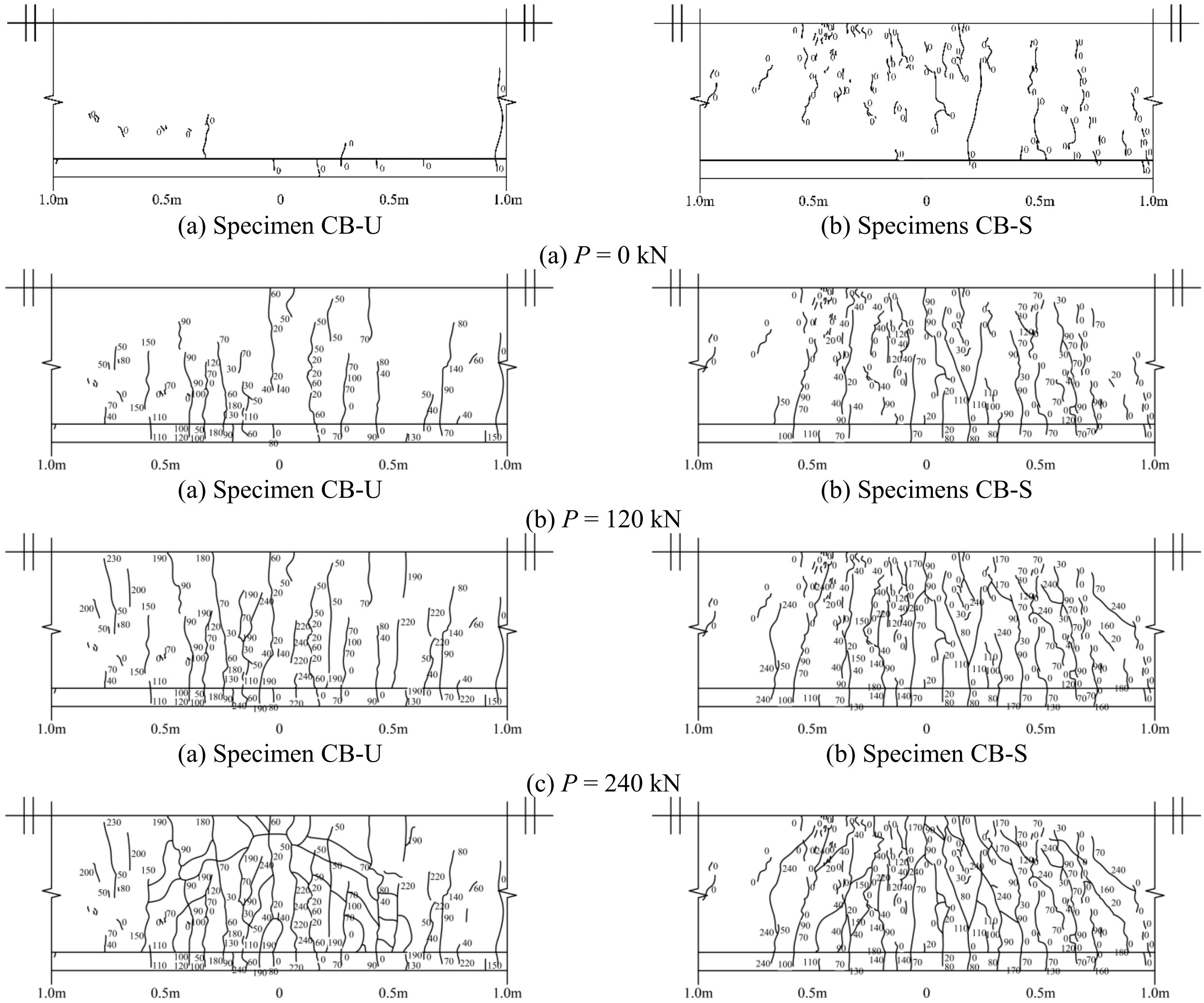

(a) Specimen CB-U (b) Specimens CB-S

(a) P = 0 kN

(a) Specimen CB-U (b) Specimens CB-S

(b) P = 120 kN

(a) Specimen CB-U (b) Specimen CB-S

(c) P = 240 kN

(a) Specimen CB-U (b) Specimen CB-S

(d) After structure failure

Fig. 16 Comparison of crack patterns of Specimens CB-U and CB-S

occurrence of cracks in the concrete slabs. Comparing the cracking state after the structural failure of Specimen CB-S, it can be clearly seen that the number of cracks in Specimen CB-U was fewer and the cracks also distributed in a more sparse pattern.

4.5 Interface slip analysis

Due to the application of foamed plastics with lower material strength around the screw and nut of the URSP-S connectors, the interface slip between the steel beam and concrete slab is permitted. Additionally, the interface slip will be significantly influenced by the URSP-S connectors arranged along the top flange of the steel beam.

Due to the geometric symmetry of Specimens SB-U, CB-U and CB-S, the displacement meters for measuring the interface slip were arranged in the half-span of the tested composite beam. The measured slip distributions and load-slip curves corresponding to Specimens SB-U, CB-U and CB-S are illustrated in Figs. 17 and 18, respectively. It can be observed from Fig. 17 that slip increased with the increment of negative loads at the initial loading stage. Moreover, dramatical enlargement of the interface slip was observed once the tested specimens were loaded to plastic stages, and the maximum slip was about 3.2 mm. Under each loading stage, the maximum interface slips uniformly occurred in the regions spacing 110 cm to the mid-span, which was close to the middle of shear span (120 cm to the mid-span).

Slip distributions and load-slip curves of Specimens CB-U and CB-S are depicted in Fig. 18. As presented in Fig. 18(a), the maximum slip occurred in negative moments region spacing from 35 cm to 85 cm to the middle span. Meanwhile, the interface slip with smaller peak value was observed in the positive moment region within the distance ranging from 260 cm to 420 cm to the middle span. The interface slip distributions tendency indicates that the slip performance of URSP-S connectors in negative moments region is insignificantly affected by the studs in positive moment region since the stud is flexible and the slip restraint is limited. As shown in Figs. 18(a) and 18(b), it can be concluded that the slip of stud is influenced by the

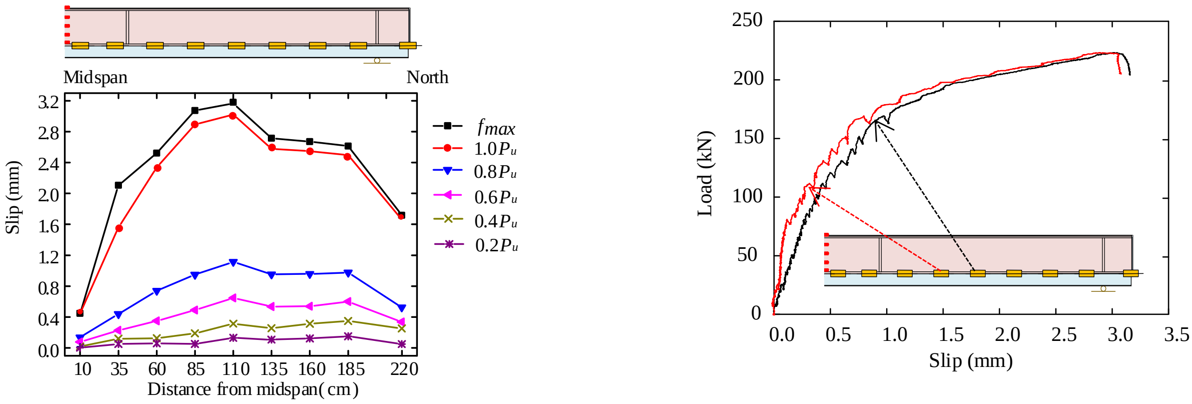

*Note: f_{max} is the maximum midspan deflection

(a) Slip distribution of Specimen SB-U (b) Load-slip behavior of Specimen SB-U

Fig. 17 Slip analysis of Specimen SB-U

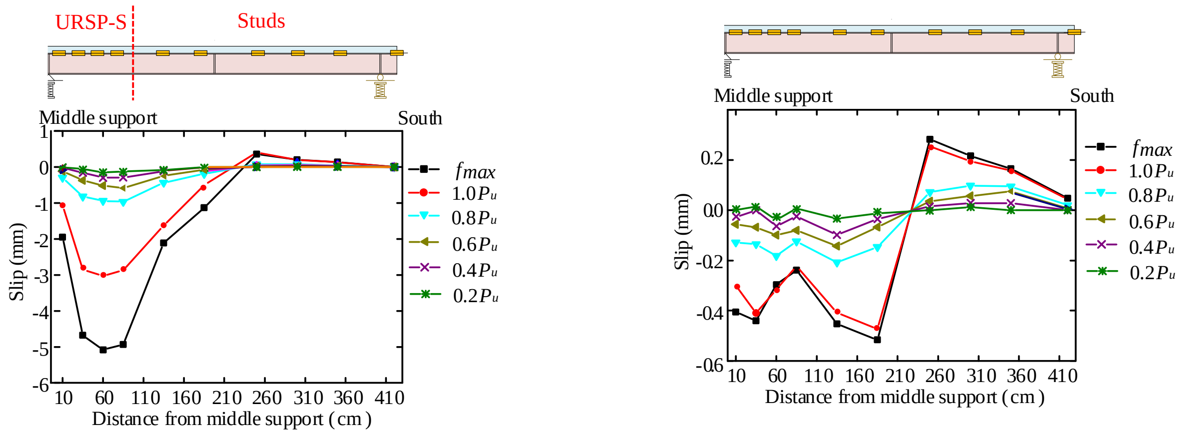

(a) Slip distribution of Specimen CB-U (b) Slip distribution of Specimen CB-S

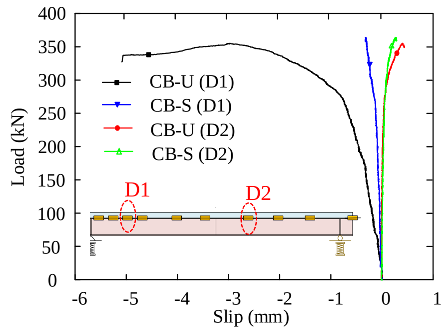

(c) Load-slip behavior of Specimens CB-U and CB-S

Fig. 18 Slip analysis of Specimens CB-U and CB-S

application of the URSP-S connector in the negative moment region, resulting in the larger slip at the interface with stud (distance from middle support was between 100 cm to 420 cm). Fig. 18(c) shows the slips measured by displacement meters D1 and D2, which correspond to the locations of the maximum slips in Specimens CB-U and CB-S, respectively. Due to the arrangement of URSP-S connectors, the slip of CB-U was much larger than CB-S at D1. Though both studs were arranged at D2 in Specimens CB-U and CB-S, the slip of CB-U was still larger than CB-S. Additionally, the overall interface slip of steel-concrete interface connected with URSP-S connectors was about 10 times larger than that with normal studs only. The experimental observations indicated that the URSP-S connectors are helpful for improving slip performance. As exhibited in Fig. 17, the large slip in the simply supported beam SB-U can also be observed.

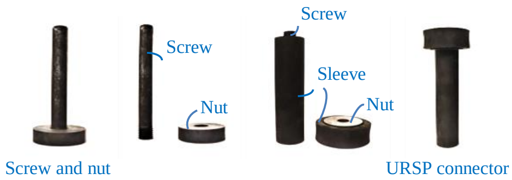

(a) Manufacture process of URSP-S connector for practical engineering

(b) Xingwei and Huangtian Overpass of 107 National Road

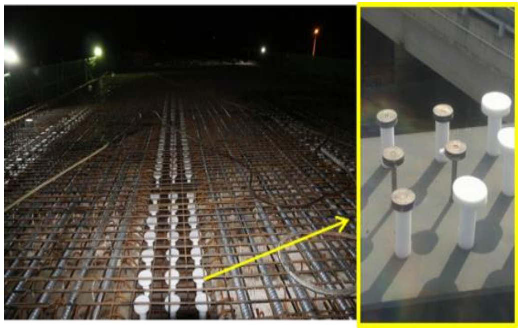

(c) Majiahu Overpass

Fig. 19 URSP-S connectors in practical engineering

The uplift or separation between the concrete slab and the steel beam is an important parameter of the shear connector. However, in this study, the uplift force was very small and the uplift bearing capacity was sufficient in the experiments. The experimental study on the uplift performance of URSP-S connectors has been reported by Nie and Ma (Nie and Ma 2015), which is hereby excluded in this study.

5. Arrangement suggestions for URSP-S connectors and engineering application

For simplifying the structure design and considering the construction convenience, the URSP-S connectors in the continuous composite beam are suggested to be arranged within the $L/4$ length range on both sides of the intermediate support, where L is the span on both sides of the support. In addition, for continuous composite beams that require higher bending stiffness, the arrangement length of the URSP-S connectors can also be appropriately shortened. However, it is recommended to be higher than $L/8$, so as to guarantee that the non-shearing effect led by the URSP-S connectors can be effectively exerted.

It is worth mentioning that due to the application of the URSP-S connectors, the shear resistance of the interface will reduce to a certain extent, and the overall bending stiffness of the composite beam becomes slightly lower as well. Meanwhile, brittle failure of the composite beams may be induced by stud shearing if the partial shear connection is adopted. Therefore, the partial shear connection should be avoided and the full shear connection is preferred to calculate the required number of connectors in each shear span.

In practical engineering, the required number of connectors is huge, the method of manufacturing the URSP-S connectors in the tests shown in Fig. 4 is time-consuming and laborious. Therefore, a more efficient approach is proposed to manufacture URSP-S connector, as shown in Fig. 19(a). Sleeves made in the low elastic modulus material can be prefabricated at the factory according to the actual size of the screw and the nut of the URSP-S connector. At the construction site, simply unscrew the nut from the screw, then cover the screw and the nut with the prefabricated sleeve, and finally tighten the nut onto the screw. The URSP-S connectors have been applied in the engineering design of Xingwei and Huangtian Overpass of 107 National Road and Majiahu Overpass in China, Figs. 19(b) and 19(c) show the URSP-S connectors arranged in hogging moment regions, the engineering results present sufficient crack resistance and the maximum tensile stress in the concrete deck is also effectively controlled. The composite beams in the aforementioned projects have exhibited satisfying crack resistance performance until now.

It has to be noted that the labor cost for installing the URSP connectors is slightly higher than that of stud connectors due to its relatively complex fabrication process. However, URSP connectors can efficiently reduce the expenses for improving the crack resistance of steel-concrete beams using conventional shear studs and the maintenance cost after cracking. Based on current engineering practices, the labor cost for installing the URSP connectors is acceptable and it can be significantly reduced with special wrapping equipment in the future.

6. Conclusions

In this study, the structural behavior of steel-concrete composite beams with URSP-S connectors was experimentally investigated. Three composite beams, including one simply supported beam under negative loading, and two two-equal-span continuous beams under loading at mid-span, were designed and tested. The failure modes, crack evolution process, ultimate capacities, strain responses at different locations as well as the interface slip of tested specimens were measured and evaluated. Based on the experimental results, the following conclusions were made:

- The application of URSP-S connectors in the negative moment region slightly decreased the overall stiffness and ultimate bearing capacity of the composite beam.
- After applying the URSP-S connectors in negative moment region, the crack width was much smaller, and the development speed of cracks became slower than the beam arranged with normal studs.
- The URSP-S connectors efficiently improved the interface slip performance. The studs in the positive moment region had limited influence on the slip performance of URSP-S connectors.
- Scientific arrangement suggestions for URSP-S connectors are proposed to guide the structural design of composite structures using URSP-S.

For extending the practical application of URSP connectors in civil engineering, further researches including the experimental analyses and finite element simulations on the force transfer mechanism and failure pattern of URSP-S connectors in various steel-concrete composite components will be performed in the follow-up studies.

Acknowledgments

The authors gratefully acknowledge the financial support provided by the National Key Research Program of China (Grant No. 2018YFC0705704), Key Research Program of China Railyway Corp. (Grant No. K2018G018) and Development Plan of Science and Technology Research of China Railway Corp. (Grant No. N2018G069).

References

Abe, H. and Nakajima, A. (1990), "Division of slabs and development of flexible connectors", *IABSE Symposium Report*, **60**, 107-112.

Bazant, Z.P. and Oh, B.H. (1983), "Deformation of cracked net-reinforced concrete walls", *J. Struct. Eng.*, **109**, 93-108. https://doi.org/10.1061/(asce)0733-9445(1983)109:1(93).

Betti, R. and Gjelsvik, A. (1996), "Elastic composite beams", *Comput. Struct.*, **59**, 437-451. https://doi.org/10.1016/0045-7949(95)00275-8.

Bursi, O.S. and Gramola G. (2000), "Behavior of composite substructures with full and partial shear connection under quasi-static cyclic and pseudo-dynamic displacements", *Mater. Struct.*, **33**(3), 154-163. https://doi.org/10.1007/BF02479409.

Dezi, L., Gara, F., Leoni, G. and Tarantino, A.M. (2001), "Time-dependent analysis of shear-lag effect in composite beams", *J. Eng. Mech.*, **127**(1), 71-79. https://doi.org/10.1061/(ASCE)0733-9399(2001)127:1(71).

Duan, L.L., Nie, X., Ding, R. and Zhuang, L.D. (2019), "Research on Application of Uplift-Restricted Slip-Permitted (URSP) Connectors in Steel-Concrete Composite Frames", *Appl. Sci.*, **9**(11), 2235. https://doi.org/10.3390/app9112235.

Ellobody, E. and Lam, D. (2002), "Modeling of headed stud in steel-precast composite beams", *Steel Compos. Struct.*, **2**(5), 355-378. https://doi.org/10.12989/scs.2002.2.5.355.

GB/T 10433-2002 (2002), Cheese head studs for arc stud welding. (in Chinese)

GB 50010-2010 (2010), Code for design of concrete structures. (in Chinese)

GB/T 228-2010 (2010), Metallic materials-tensile testing-method of test at ambient temperature. (in Chinese)

GB/T 6478-2015 (2015), Steels for cold heading and cold extruding. (in Chinese)

GB/T JFJ138-2016 (2016), Code for design of composite structures.(in Chinese)

GB/T 50081-2016 (2016), Standard for test method of mechanical properties on ordinary concrete. (in Chinese)

Han, S.W. Experimental Study on Steel-Concrete Composite Beam with Uplift-Restricted and Slip-Permitted Connectors. Master's Degree, Tsinghua University, Beijing, China, 2016. (In Chinese)

Hajjar, J.F. (1998), "A distributed plasticity model for concrete-filled steel tube beam columns with interlayer slip", *Eng. Struct.*, **20**(8), 663-676. https://doi.org/10.1016/S0141-0296(97)00107-7.

He, S.H., Fang, Z., Fang, Y.W., Liu, M., Liu, L.Y. and Ayman, S.M. (2016), "Experimental study on perfobond strip connector in steel–concrete joints of hybrid bridges", *J. Constr. Steel Res.*, **118**, 169-179. https://doi.org/10.1016/j.jcsr.2015.11.009.

Hsu, C.T.T., Punurai, S. and Punurai, W. (2014), "New composite beams having coldformed steel joists and concrete slab", *Eng. Struct.*, **71**(15), 187-200. https://doi.org/10.1016/j.engstruct.2014.04.011.

Huang, Y., Yi, W.J. and Nie, J.G. (2012), "Seismic analysis of CFST frames considering the effect of the floor slab", *Steel Compos. Struct.*, **13**(4), 397-408. https://doi.org/10.12989/scs.2012.13.4.397.

Johnson R P. (2004), "Composite structures of steel and concrete, Vol. 1: Beams, columns, frames and applications in building". 3rd Ed. Oxford: Blackwell Scientific.

Lam, D. and Williams, C.A. (2004), "Experimental study on concrete filled square hollow sections", *Steel Compos. Struct.*, **4**(2), 95-112. https://doi.org/10.12989/scs.2004.4.2.095.

Li, Z.Y., Tao, M.X., Nie, J.G. and Fan, J.S. (2017), "Analysis and optimization of a continuous composite bridge with uplift-restricted and slip-permitted connectors", *IABSE Symposium Report.* Zurich, Switzerland, September.

Li, Z.Y., Ma X.W., Fan, J.S. and Nie, X. (2019), "Overhanging tests of steel–concrete composite girders with different connectors", *J. Bridge Eng.*, **24**(11), 04019098. https://doi.org/10.1061/(ASCE)BE.1943-5592.0001481.

Liang, Q.Q., Uy, B., Bradford, M.A. and Ronagh, H.R. (2004). Ultimate strength of continuous composite beams in combined bending and shear. *J. Constr. Steel Res.*, **60**(8), 1109-1128. 10.1016/j.jcsr.2003.12.00110.1016/j.jcsr.2003.12.001

Liu, X.G., Fan, J.S., Bai, Y., Tao, M.X. and Nie, J.G. (2015), "Stress increment of unbonded prestressing tendons in prestressed concrete girders with corrugated steel webs", *J. Bridge Eng.*, **20**(7), 040140941-11. https://doi.org/10.1061/(ASCE)BE.1943-5592.0000694.

Liu, Y., Guo, L. and Qu, B. (2017), "Experimental investigation on the flexural behavior of steel-concrete composite beams with U-shaped steel girders and angle connectors", *Eng. Struct.*, **131**(15), 492-502. https://doi.org/10.1016/j.engstruct.2016.10.037.

Martinelli, E., Faella, C. and Palma, G.D. (2012), "Shear-flexible steel-concrete composite beams in partial interaction: closed-form 'exact' expression of the stiffness matrix", *J. Eng. Mech.*, **138**(2), 151-163. https://doi.org/10.1061/(ASCE)EM.1943-7889.0000320.

Mirza, O. and Uy, B. (2010), "Finite element model for the long-term behaviour of composite steel-concrete push tests", *Steel*

Compos. Struct., **10**(1), 45-67. https://doi.org/10.12989/scs.2010.10.1.045.

Nguyen, G.B. and Machacek, J. (2016), "Effect of local small diameter stud connectors on behavior of partially encased composite beams", *Steel Compos. Struct.*, **20**(2), 251-266. https://doi.org/10.12989/scs.2016.20.2.251.

Nie, J.G., Li, Y.X., Tao, M.X. and Nie, X. (2015), "Uplift-restricted and slip-permitted T-Shape connectors", *J. Bridge Eng.*, **20**(4), 04014073. https://doi.org/10.1061/(ASCE)BE.1943-5592.0000660.

Nie, J.G., Ma, Y. (2015), "The experimental study of the uplift performance of uplift-restricted and slip-permitted screw-type connectors", *Special Struct.*, **32**(3), 6-12. (in Chinese)

Nie, J.G., Wang, J.J. and Gou, S.K. (2019), "Technological development and engineering applications of novel steel-concrete composite structures", *Front. Struct. Civ. Eng.*, **13**(1), 1-14. https://doi.org/10.1007/s11709-019-0514-x.

Oguejiofor, E.C. and Hosain, M. (1994), "A parametric study of perfobond rib shear connectors", *Can. J. Civil. Eng*., **21**(4), 614-625. https://doi.org/10.1139/l94-063.

Okumus, P., Oliva, M.G. and Becker, S. (2012), "Nonlinear finite element modeling of cracking at ends of pretensioned bridge girders", *Eng. Struct.*, **40**, 267-275. https://doi.org/10.1016/j.engstruct.2012.02.033.

Ollgaard, J.G., Slutter, R.G. and Fishe, J.W. (1971), "Shear strength of stud connectors in lightweight and normal - weight concrete", *AISC Eng. J. Am. Inst. Steel Constr.*, **169**(8), 55-64.

Park, R. and Thompson, K.J. (1974), "Behavior of prestressed, partially prestressed, and reinforced concrete interior beam-column assemblied under cyclic loading: test results of units 1 to 7", Research Report 74-9, Dept. of Civil Engineering, University of Canterbury, Chrischurch, New Zealand.

Prodyot, K.B., Alfarabi, M.S. and Nesar, U.A. (1987), "Partially prestressed continuous composite beams I", *J. Struct. Eng.*, **113**(9), 199-1925. https://doi.org/10.1061/(ASCE)0733-9445(1987)113:9(1909).

Ranzi, G., Bradford, M.A. and Uy, B. (2004), "A direct stiffness analysis of a composite beam with partial interaction". *Int. J. Numer. Meth. Eng.*, **61**(5), 657-672. https://doi.org/10.1002/nme.1091.

Seracino, R., Oehlers, D.J. and Yeo, M.F. (2001), "Partial-interaction flexural stresses in composite steel and concrete bridge beams", *Eng. Struct.*, **23**(9), 1186-1193. https://doi.org/10.1016/S0141-0296(00)00121-8.

Song, G., Mo, Y.L., Otero, K. and Gu, H. (2006), "Health monitoring and rehabilitation of a concrete structure using intelligent materials", *Smart Mater. Struct.*, **15**, 309-314. https://doi.org/10.1088/0964-1726/15/2/010.

Suwaed, A.S.H. and Karavasilis, T.L. (2017), "Novel Demountable shear connector for accelerated disassembly, repair, or replacement of precast steel-concrete composite bridges", *J. Bridge Eng.*, **22**(9), 04017052. https://doi.org/10.1061/(ASCE)BE.1943-5592.0001080.

Suwaed, A.S.H. and Karavasilis, T.L. (2018), "Removable shear connector for steel-concrete composite bridges", *Steel Compos. Struct.*, **29**(1), 107-123. https://doi.org/10.12989/scs.2018.29.1.107.

Taeyang, Y. (2004), "Static behavior of large stud shear connectors", *Eng. Struct.*, **26**(12), 1853-1860. https://doi.org/10.1016/j.engstruct.2004.07.011.

Taranath, B.S. (2011), "Structural Analysis and Design of Tall Buildings: Steel and Composite Construction", Crc Press, Boca Raton, FL.

Wegmuller, A.W. and Amer, H.N. (1977), "Nonlinear response of composite steel-concrete bridges", *Compos. Struct.*, **7**(2), 161-169. https://doi.org/10.1016/0045-7949(77)90033-5.

DL